Direct, on-the-fly calculation of unresolved resonance region cross sections in Monte Carlo simulations

ANS MC2015 - Joint International Conference on Mathematics and Computation (M&C), Supercomputing in Nuclear Applications (SNA) and the Monte Carlo (MC) Method · Nashville, Tennessee · April 19–23, 2015, on CD-ROM, American Nuclear Society, LaGrange Park, IL (2015)

DIRECT, ON-THE-FLY CALCULATION OF UNRESOLVED RESONANCE REGION CROSS SECTIONS IN MONTE CARLO SIMULATIONS

Jonathan A. Walsh, Benoit Forget, and Kord S. Smith
Department of Nuclear Science and Engineering
Massachusetts Institute of Technology
77 Massachusetts Avenue, 24-107
Cambridge, MA 02139
walshjon@mit.edu; bforget@mit.edu; kord@mit.edu

Brian C. Kiedrowski* **and Forrest B. Brown**
XCP-3, Monte Carlo Codes
Los Alamos National Laboratory
Los Alamos, NM 87545
bckiedro@lanl.gov; fbrown@lanl.gov

ABSTRACT

The theory, implementation, and testing of a method for on-the-fly unresolved resonance region cross section calculations in continuous-energy Monte Carlo neutron transport codes are presented. With this method, each time that a cross section value is needed within the simulation, a realization of unresolved resonance parameters is generated about the desired energy and temperature-dependent single-level Breit-Wigner resonance cross sections are computed directly via use of the analytical $\psi - \chi$ Doppler integrals. Results indicate that, in room-temperature simulations of a system that is known to be highly sensitive to the effects of resonance structure in unresolved region cross sections, the on-the-fly treatment produces results that are in excellent agreement with those produced with the well-established probability table method. Additionally, similar agreement is observed between results obtained from the on-the-fly and probability table methods for another intermediate spectrum system at temperatures of 293.6 K and 2500 K. With relatively tight statistical uncertainties at the ~ 10 pcm level, all on-the-fly and probability table k_{eff} eigenvalues agree to within 2σ. Also, we use the on-the-fly approach to show that accounting for the resonance structure of competitive reaction cross sections can have non-negligible effects for intermediate/fast spectrum systems. Biases of up to 90 pcm are observed. Finally, the consequences of the on-the-fly method with respect to simulation runtime and memory requirements are briefly discussed.

Key Words: Nuclear Data, Cross Sections, Unresolved Resonance Region, Doppler Broadening, Monte Carlo

1 INTRODUCTION

The use of Monte Carlo particle transport codes, which, in principle, allow for physical and geometrical models of arbitrary fidelity, has historically been limited by the availability of computational resources. However, with the increased processing power of modern high-performance

*Currently at the University of Michigan: bckiedro@umich.edu.

computing (HPC) platforms, Monte Carlo methods are increasingly being considered for practical reactor analysis, rather than simply benchmarking purposes. Future research and development efforts will benefit from improved computational methods for the representation of nuclear data in Monte Carlo simulations of advanced reactor systems, many of which rely on intermediate or fast neutron energy spectra. For the simulation and analysis of fast reactors, and also the critical assemblies that are used for validation of nuclear data and computational methods, the treatment of neutron cross sections in the unresolved resonance energy region is especially important. And while future reliance on cumbersome legacy nuclear data preparation procedures will likely be reduced by promising methods for on-the-fly* processing of thermal scattering data [1] and resolved resonance energy region cross sections [2–4], the treatment of unresolved resonance region data has received less attention in recent decades. A high-fidelity, memory-reducing on-the-fly method for generating unresolved resonance region neutron cross sections in Monte Carlo transport simulations is the focus of this work.

In this section we give brief introductions to important physical phenomena that characterize the unresolved resonance energy region and the computational methods that have typically been employed for capturing the effects of those phenomena in Monte Carlo simulations. Section 1.1 highlights defining characteristics of the unresolved resonance region as applicable to neutron transport simulations. In Sec. 1.2 we describe the use of so-called infinite-dilute cross sections in the unresolved resonance region and the pitfalls of this approach. The probability table method for treating resonance cross section structure in the unresolved region is briefly outlined in Sec. 1.3 and Sec. 1.4 discusses the importance of accounting for the resonance structure of competitive reaction cross sections. In Sec. 2 we explain the on-the-fly method of generating cross sections in the unresolved resonance region. Results obtained with the on-the-fly method are presented in Sec. 3 along with results obtained with the infinite-dilute and probability table methods. Conclusions reached in this initial study and areas for future research are discussed in Sec. 4.

1.1 Unresolved Resonance Region

At sufficiently high incident neutron energies, on average, individual resonances become broader, exhibit lower peak values, and are spaced close enough together that they overlap significantly with one another. In this region, the localized structure of a single resonance is insignificant relative to the collective structure of several resonances spanning a wider energy range. The energies that are characterized by this sort of cross section behavior comprise the fast energy region [5]. The fast energy region boundaries for different nuclides will vary with the onset coming at lower energies for heavier nuclides than for lighter ones. At somewhat lower incident neutron energies, the resonances for a given nuclide will be narrower, more pronounced, and better separated from neighboring resonances. These properties make individual resonances more easily distinguishable from one another in cross section measurement experiments. That is, the resonances can be resolved experimentally. Unlike in the fast energy region, there is sharp structure associated with individual resonances at these energies and this structure must be carefully accounted for in neutron transport simulations. Energies characterized by this type of behavior make up the resolved resonance

*We use the term *on-the-fly* to describe methods which perform the calculation of some value within the simulation, rather than those which utilize values that are pre-computed prior to the initialization of a simulation.

region [5]. The intermediate incident neutron energies between the resolved resonance and fast energy regions make up the unresolved resonance region (URR). In the URR, individual resonances cannot all be resolved experimentally even though, in reality, single resonances exhibit distinct structure, just as in the resolved resonance region. As a result, precise cross section values are unknown in the URR. Instead of precise descriptions of URR resonances and cross sections, we must rely on average descriptions and statistical distributions [5].

1.2 Averaged, Infinite-dilute Cross Sections

Though precise cross section values at any given incident neutron energy, E_n, in the URR are unknown, based on mean unresolved resonance parameter values and the statistical distributions of those values, we can construct the probability distribution, $P(\sigma_r'|E_n)$, of cross section values for reaction r. Then we can write an expression for the expected cross section value as a Lebesgue integral in σ_r'-space,

$$\langle \sigma_r(E_n) \rangle = \int_{-\infty}^{\infty} d\sigma_r' P(\sigma_r'|E_n)\sigma_r'. \tag{1}$$

This averaged, expected value is what is commonly referred to as an infinite-dilute cross section. Historically, in the absence of precisely known URR resonance structure, these expected cross sections were used in Monte Carlo neutron transport simulations.

Use of the infinite-dilute cross sections, though, is tantamount to neglecting energy self-shielding effects. By obtaining expected cross section values in the manner just described, we have smoothed out the resonance structure of the URR. That is, in the narrow energy intervals where resonances actually occur, we have a reduced value, and in the wider energy intervals between real URR resonances, we have an increased value. So, over the majority of URR energies, infinite-dilute cross sections are greater than the unknown, precise values. It is known that this phenomenon leads to significant over-predictions of reaction rates, notably capture by resonant absorbers (e.g. ^{238}U) in intermediate energy spectrum systems when infinite-dilute cross sections are used in simulations. This can result in under-predicted, non-conservative k_{eff} eigenvalue calculations [6].

1.3 Probability Tables

In order to more faithfully account for resonance structure and the resulting self-shielding effects in the URR — phenomena that can be worth hundreds of pcm in intermediate spectrum systems — the probability table method was proposed [7]. This method relies on the sampling of discrete cross section values with associated discrete probabilities such that, in the limit of many samples, the expected cross section value at a given E_n is preserved. Although expected cross sections are preserved, the distribution of discrete cross section-probability pairs provides a more realistic model for URR self-shielding effects. Probability tables are generated in a pre-processing step before the start of a neutron transport simulation. In general, a different set of tables is required at every temperature, for each nuclide with a URR, in a simulation. Certain practical considerations in implementing the probability table method are well-documented [8–10].

1.4 Competitive Reaction Cross Section Resonance Structure

Though there may be multiple competing reactions at URR energies, the ENDF-6 format [11] allows the specification of File 2 unresolved resonance parameters for only elastic scattering, radiative capture, fission, and a single competitive reaction, typically inelastic scattering to the first excited level of the compound nucleus, if energetically possible. Any resonance structure in another reaction must be entirely described via pointwise energy-cross section pairs in File 3[†].

Further, despite allowing for the specification of URR resonance parameters for a competitive reaction, the ENDF-6 format prescribes the use of only the File 3 averaged cross section values. The possibility of different treatments of the competitive reaction cross section inducing biases in simulation results is mentioned by MacFarlane, et. al [12]. In their code-to-code comparison study of Big Ten critical assembly simulations, it is noted that the TRIPOLI code [13], in making use of URR cross section data generated with the CALENDF nuclear data processing code [14], accounts for resonance structure in the competitive reaction cross section. Many other transport codes, such as MCNP [15], utilize the infinite-dilute URR cross section values that are produced by the NJOY Nuclear Data Processing System [16]. Here, in OpenMC [17], we have isolated competitive reaction cross section resonance structure effects by allowing for the on-the-fly use of either averaged or structured values.

2 ON-THE-FLY CROSS SECTION CALCULATIONS

In this section we describe the on-the-fly method of generating URR cross sections. The method is implemented in the OpenMC neutron transport code [17]. The sampling of unresolved resonance parameters and use of the sampled parameters in cross section computations using the single-level Breit-Wigner formulae are discussed in Secs. 2.1 and 2.2, respectively. Notation for selected variables is given in Appendix A.

2.1 Level Spacings and Partial Widths

In the energy region about any incident neutron laboratory system energy, E_n, at which we wish to compute a realization of URR cross section values, we must statistically generate an ensemble of resonances. This ensemble, sometimes referred to as a resonance ladder in the context of probability table generation, is determined by the energies at which resonances occur as well as the partial reaction widths characterizing each of the resonances. The process for sampling these values proceeds directly from the unresolved resonance parameters given in File 2 of an ENDF-6 format [11] evaluated nuclear data file.

We are first concerned with the mean unresolved resonance parameter values given for an individual spin sequence which is defined by an orbital angular momentum quantum number, l, and a total angular momentum quantum number, J. There are N_l orbital quantum numbers associated

[†]Any structure that is represented in the File 3 background cross section is typically quite crude because it is only the gross structure over multiple URR resonances, not the structure of individual resonances.

with the URR for a given nuclide. For each of these N_l values, there are $N_J(l)$ total angular momentum quantum numbers. That is, N_l is a nuclide-dependent quantity and $N_J(l)$ is dependent on both the nuclide and the l values for that nuclide.

For each (l, J) spin sequence, we sample level spacings (i.e. energy differences between adjacent resonance energies) and partial reaction widths using those parameters' mean values and their statistical distributions. The mean parameter values at a specific E_n are determined by interpolation[‡] between the values at the energies tabulated in the ENDF-6 File 2. The spread of level spacings and partial reaction widths are described by the Wigner distribution and χ^2 distributions with varying degrees of freedom, respectively. The Wigner distribution for level spacings is given by

$$P_W\left(\frac{D^{l,J}(E_n)}{\langle D^{l,J}(E_n)\rangle}\right) = \frac{\pi D^{l,J}(E_n)}{2\langle D^{l,J}(E_n)\rangle}\exp\left(-\frac{\pi D^{l,J}(E_n)^2}{4\langle D^{l,J}(E_n)\rangle^2}\right). \tag{2}$$

Direct sampling of this distribution gives

$$D^{l,J}(E_n) = \langle D^{l,J}(E_n)\rangle\sqrt{-4\log(\xi)/\pi}, \tag{3}$$

for a random number on the unit interval, ξ. Partial widths for reaction r, Γ_r, are obtained by sampling a χ^2 distribution,

$$P_{\chi^2(\mu_r)}(y) = \frac{\exp\left(-\frac{y}{2}\right)y^{\frac{\mu_r}{2}-1}}{2^{\mu_r/2}G\left(\frac{\mu_r}{2}\right)}; \qquad y \equiv \mu_r\frac{\Gamma_r^{l,J}}{\langle\Gamma_r^{l,J}(E_n)\rangle} \tag{4}$$

with a reaction channel-dependent number of degrees of freedom, $\mu_r(l, J)$. The $G\left(\frac{\mu_r}{2}\right)$ term in Eq. (4) is the Gamma function.

With a sample y and the mean parameter values and degrees of freedom provided in an ENDF-6 file, it is straightforward to obtain sample partial widths for radiative capture, $\Gamma_\gamma^{l,J}$; fission, $\Gamma_f^{l,J}$; and the single competitive reaction, $\Gamma_x^{l,J}$. The energy-dependent sampled neutron width is then calculated as

$$\Gamma_n^{l,J}(E_n) = \nu_l(E_n)\sqrt{E_n}\langle\Gamma_{n,0}^{l,J}\rangle\mu_n\frac{\Gamma_{n,0}^{l,J}}{\langle\Gamma_{n,0}^{l,J}\rangle} \tag{5}$$

using a mean reduced neutron width value, $\langle\Gamma_{n,0}^{l,J}\rangle$. The derived variables ν_l and ρ are given by P_l/ρ and $a_c k(E_n)$, respectively. In these expressions, a_c, k, and P_l are the channel radius, center-of-mass neutron wavenumber, and orbital quantum number-dependent penetration factor, respectively. The procedures for computing the channel radius and a related quantity, the scattering radius, a_s, are detailed in the ENDF-6 Formats Manual [11]. The wavenumber is given by

$$k(E) = \frac{10\sqrt{2m_n}}{\hbar c}\frac{A}{A+1}\sqrt{|E|} \tag{6}$$

with m_n, $\hbar c$, and A being the mass of a neutron in eV, the reduced Planck constant multiplied by the speed of light in eV-fm, and the ratio of the mass of the target nuclide to that of a neutron, respectively.

[‡]The nuclide-dependent interpolation scheme is prescribed in the ENDF-6 file.

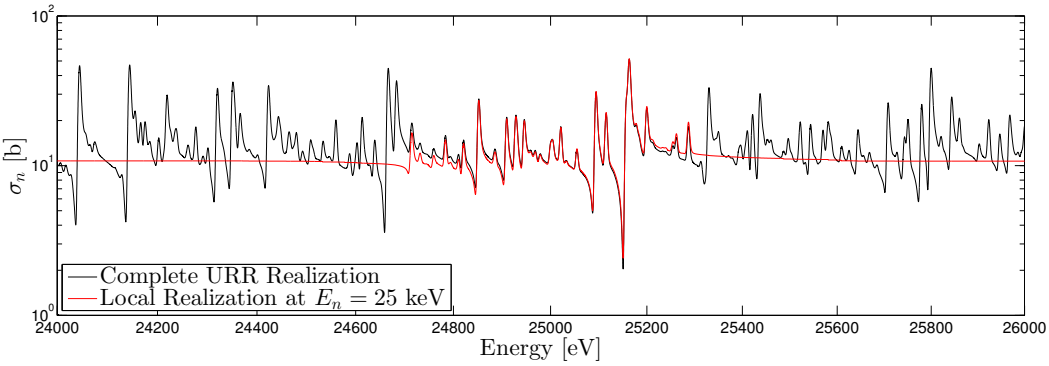

Figure 1. ^{238}U Elastic Scattering Cross Section Realization About $E_n = 25$ keV for $N_\lambda = 64$

2.2 Single-level Breit-Wigner Cross Sections

From the sampled level spacings and partial reaction widths, cross section values at a given E_n are computed using a so-called many-level Breit-Wigner model[§] [18]. In this model, a cross section at E_n is computed as a summation of the contributions from each of N_λ single-level Breit-Wigner (SLBW) resonances [19] to the value at this energy. The value of N_λ must be chosen, for each spin sequence, to be high enough that the addition of a nominal resonance's contribution to the cross section values at E_n is negligible. Initial studies suggest that an N_λ value of 64 will produce satisfactory differential and integral results for the range of systems investigated here. This determination is based on the observations that the resulting partial reaction cross section values are unbiased at the 0.1% relative difference level when compared to values computed using a higher N_λ value and that the k_{eff} values that are computed in simulations using cross section realizations generated with 64 contributing resonances from each spin sequence are unbiased relative to the results that are obtained with additional resonances. To illustrate, the schematic in Fig. 1 shows a realization of the ^{238}U elastic scattering cross section localized about $E_n = 25$ keV along with the full realization. It is apparent that the truncated, local realization is sufficient to capture resonance cross section structure in the vicinity of the desired energy. Each time that a cross section value is needed within a simulation, the on-the-fly calculation method requires a new generation of an independent realization localized about E_n. The SLBW elastic neutron scattering cross section is given by

$$\begin{aligned}\sigma_n(E_n) &= \sigma_{\text{pot}}(E_n) \\ &+ \sum_{l=0}^{N_l-1} \sum_{j=1}^{N_J(l)} \sum_{\lambda=1}^{N_\lambda} \sigma_\lambda \left(\left[\cos\left(2\phi_l(E_n)\right) - \left(1 - \frac{\Gamma_{n,\lambda}}{\Gamma_\lambda}\right) \right] \psi(\theta, x) + \chi(\theta, x) \sin\left(2\phi_l(E_n)\right) \right).\end{aligned} \tag{7}$$

The potential, or shape elastic, scattering cross section appears in the above expression and is calculated as

$$\sigma_{\text{pot}}(E_n) = \frac{4\pi}{k^2(E_n)} \sum_{l=0}^{N_l-1} (2l+1) \sin^2\left(\phi_l(E_n)\right). \tag{8}$$

[§]This many-level Breit-Wigner model should not be confused with the multi-level Breit-Wigner (MLBW) resonance formalism.

It is well-known that, due to its neglect of level-level interference effects, the SLBW representation can result in unphysical negative elastic scattering cross sections. When a negative value is encountered, the elastic scattering cross section is simply set to zero in our implementation. This adjustment is propagated through to the total cross section which is calculated as the sum of partial reaction values.

Radiative capture, fission, and the competitive reaction cross sections are given by

$$\sigma_\gamma(E_n) = \sum_{l=0}^{N_l-1} \sum_{j=1}^{N_J(l)} \sum_{\lambda=1}^{N_\lambda} \sigma_\lambda \frac{\Gamma_{\gamma,\lambda}}{\Gamma_\lambda} \psi(\theta, x), \tag{9}$$

$$\sigma_f(E_n) = \sum_{l=0}^{N_l-1} \sum_{j=1}^{N_J(l)} \sum_{\lambda=1}^{N_\lambda} \sigma_\lambda \frac{\Gamma_{f,\lambda}}{\Gamma_\lambda} \psi(\theta, x), \tag{10}$$

and

$$\sigma_x(E_n) = \sum_{l=0}^{N_l-1} \sum_{j=1}^{N_J(l)} \sum_{\lambda=1}^{N_\lambda} \sigma_\lambda \frac{\Gamma_{x,\lambda}}{\Gamma_\lambda} \psi(\theta, x), \tag{11}$$

respectively. The total cross section is calculated as the sum of the N_r partials,

$$\sigma_{\text{tot}}(E_n) = \sum_{i=1}^{N_r} \sigma_{r,i}(E_n). \tag{12}$$

Other formulae and variables needed for the computation of cross sections include those for the neutron resonance energy, E_λ; the resonance peak value,

$$\sigma_\lambda = g_J \frac{4\pi}{k^2(E_\lambda)} \frac{\Gamma_n}{\Gamma_\lambda}; \tag{13}$$

the statistical spin factor,

$$g_J = \frac{2J+1}{4I+2}; \tag{14}$$

the neutron width evaluated at the resonance energy,

$$\Gamma_{n,\lambda}(|E_\lambda|) = \frac{\Gamma_{n,\lambda}(E_n) P_l(|E_\lambda|)}{P_l(E_n)}; \tag{15}$$

$$\theta = \frac{\Gamma_\lambda}{2\sqrt{k_{\text{B}} T E_n / A}}, \tag{16}$$

with T being the temperature of the material in which the target nuclide resides;

$$x = \frac{2(E_n - E'_\lambda)}{\Gamma_\lambda}; \tag{17}$$

and the shifted resonance energy,

$$E'_\lambda = E_\lambda + \Gamma_{n,\lambda} \frac{S_l(|E_\lambda|) - S_l(E_n)}{2P_l(|E_\lambda|)}. \tag{18}$$

Expressions for the penetrabilities, P_l; hard-sphere phase shifts, ϕ_l; and resonance energy shift factors, S_l, are given in the ENDF-6 Formats Manual [11].

Continuous-energy Doppler broadening, as opposed to the pointwise kernel broadening of the SIGMA1 method [20], is accomplished using the $\psi - \chi$ Doppler integral functions [21]. These functions are given by

$$\psi(\theta, x) = \frac{\theta\sqrt{\pi}}{2}\text{Re}\left[W\left(\frac{\theta x}{2}, \frac{\theta}{2}\right)\right] \qquad \text{and} \qquad \chi(\theta, x) = \frac{\theta\sqrt{\pi}}{2}\text{Im}\left[W\left(\frac{\theta x}{2}, \frac{\theta}{2}\right)\right], \tag{19}$$

respectively. The W-function, also known as the Faddeeva function, is defined as

$$W(\alpha, \beta) = \exp\left(-z^2\right)\text{erfc}\left(-iz\right) = \frac{i}{\pi}\int_{-\infty}^{\infty} dt \frac{\exp\left(-t^2\right)}{z - t} \tag{20}$$

with α and β being the real and imaginary components, respectively, of complex number $z = \alpha + i\beta$. With the presented procedures for sampling resonance parameters and subsequently calculating temperature-dependent cross section values, the relationship that exists between cross section values at different temperatures, for a given nuclide and fixed energy, can be preserved with relative ease. When a neutron streams into a region that contains a nuclide which was also contained in another region previously traversed by the same neutron, without any interactions in between, the cross section values in the two different regions must be related, regardless of temperature. A new set of resonances should not be generated when the neutron passes into the latter region. The same resonances should be used to compute cross sections in both regions, with any differences due to Doppler broadening only. With the on-the-fly method, this is accomplished by simply storing the set of sampled resonance parameters, generated near the current energy, between interactions and use it to compute cross sections at any required temperature. Similar functionality is possible with the probability table method [10].

As another practical point of implementation, URR cross section values, once computed, can be utilized in one of two ways. In the first case, cross section values computed from File 2 unresolved resonance parameters using the above equations are simply to be added to any background File 3 cross sections. In the second, the computed cross section values are divided by pre-computed, averaged, infinite-dilute values. The resulting factor is then multiplied by the cross section value given in File 3 to obtain the cross section value that is to be used in the transport simulation. For a given nuclide, the evaluated nuclear data file prescribes which of these treatments to use.

3 RESULTS AND ANALYSIS

In this section we present results obtained from OpenMC simulations of an infinite, homogeneous medium test problem and the Big Ten critical assembly [22]. Specifically, the *improved model* of the Big Ten system taken from the International Criticality Safety Benchmark Evaluation Project (ICSBEP) handbook [23] is used. For each system, we examine the k_{eff} eigenvalues and normalized neutron flux energy spectra that result from various URR cross section treatments. Particular attention is given to the comparison of results obtained from simulations using probability tables and on-the-fly cross sections. The effects of the treatment of the structure of the ^{238}U first

level inelastic scattering cross section on simulation results are also explicitly investigated. The infinite, homogeneous system is simulated at different temperatures to further validate the on-the-fly URR cross section Doppler broadening methodology.

All simulations are performed using the ENDF71x neutron data library [24]. Where needed, probability tables are also drawn from ENDF71x. This library contains ENDF/B-VII.1 nuclear data [25] processed into ACE format with the NJOY Nuclear Data Processing System, version 99.393 [16]. Resonance parameters and other variables required for on-the-fly cross section calculations are taken from the raw ENDF/B-VII.1 evaluations.

3.1 Infinite, Homogeneous Medium Test Problem

We start our investigation of URR cross section treatments with a simple infinite, homogeneous medium system. It is composed of a 10:1 ratio of ^{238}U and ^{235}U nuclei that is brought to critical with the addition of ^{10}B. The test problem is constructed to have an intermediate/fast neutron energy spectrum so that it is sensitive to the handling of the URR. The simplicity of the model and its relatively hard energy spectrum make it an effective system to use in the testing of the on-the-fly URR cross section calculation method. The system is simulated at both 293.6 K and 2500 K to demonstrate the consistency between cross sections broadened directly via Doppler integrals and probability table data pre-computed at a given temperature. Eigenvalue results and neutron flux energy spectra are presented in Secs. 3.1.1 and 3.1.2, respectively. In this problem, only ^{238}U and ^{235}U have a URR that must be handled. When required, on-the-fly cross sections are computed only for ^{238}U with structured ^{235}U cross sections being taken from probability tables.

Table I. Comparison of k_{eff} for Various URR Treatments at 293.6 K

URR Method	Inelastic Cross Section	k_{eff}	1σ
Averaged	Averaged	1.00001	0.00008
Probability tables	Averaged	1.00390	0.00009
On-the-fly	Averaged	1.00403	0.00008
On-the-fly	Structured	1.00493	0.00008

Table II. Comparison of k_{eff} for Various URR Treatments at 2500 K

URR Method	Inelastic Cross Section	k_{eff}	1σ
Averaged	Averaged	0.99935	0.00008
Probability tables	Averaged	1.00071	0.00008
On-the-fly	Averaged	1.00065	0.00008
On-the-fly	Structured	1.00099	0.00008

3.1.1 k_{eff} eigenvalues

In Tables I and II the k_{eff} eigenvalue results are shown for various URR treatments at 293.6 K and 2500 K, respectively. At each temperature we can see the sensitivity of the model to the

representation of cross section resonance structure. Going from the averaged cross sections to those which account for resonance structure with probability tables can result in a k_{eff} increase of hundreds of pcm. This behavior is brought on by a decrease in ^{238}U resonance absorption.

With respect to the accuracy of the on-the-fly method, we see agreement to well within 2σ between k_{eff} values computed with probability table cross sections and those computed with on-the-fly cross sections. This agreement is desired because the probability table method is essentially a discretized version of the on-the-fly method which is continuous with respect to energy, temperature, and cross section probabilities. Then, comparing the two cases in which cross sections are computed on-the-fly, there is an additional non-negligible bump in reactivity that comes when the resonance structure of the first level inelastic scattering reaction cross section is accounted for. This increase amounts to approximately 90 pcm and 30 pcm at 293.6 K and 2500 K, respectively.

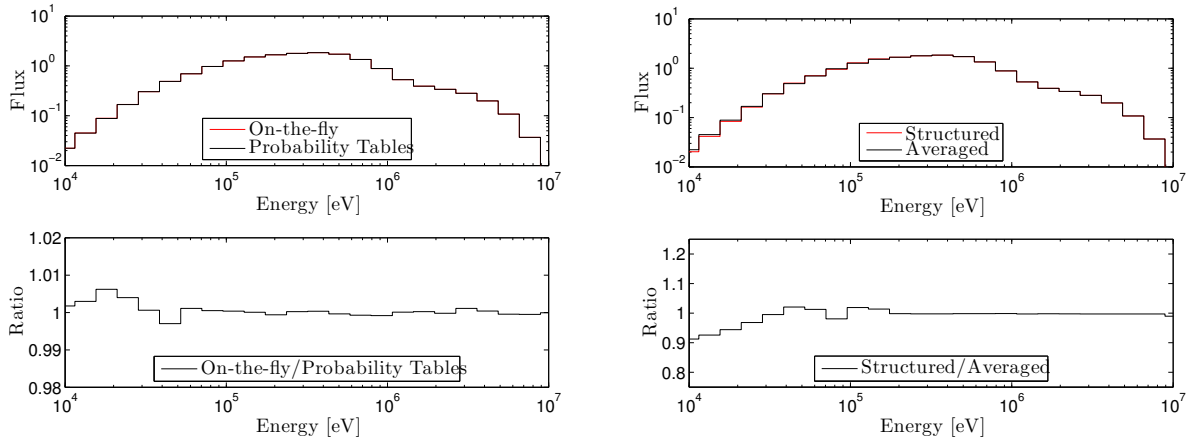

(a) On-the-fly & Probability Tables **(b) Structured & Averaged**

Figure 2. Flux Spectra at 293.6 K

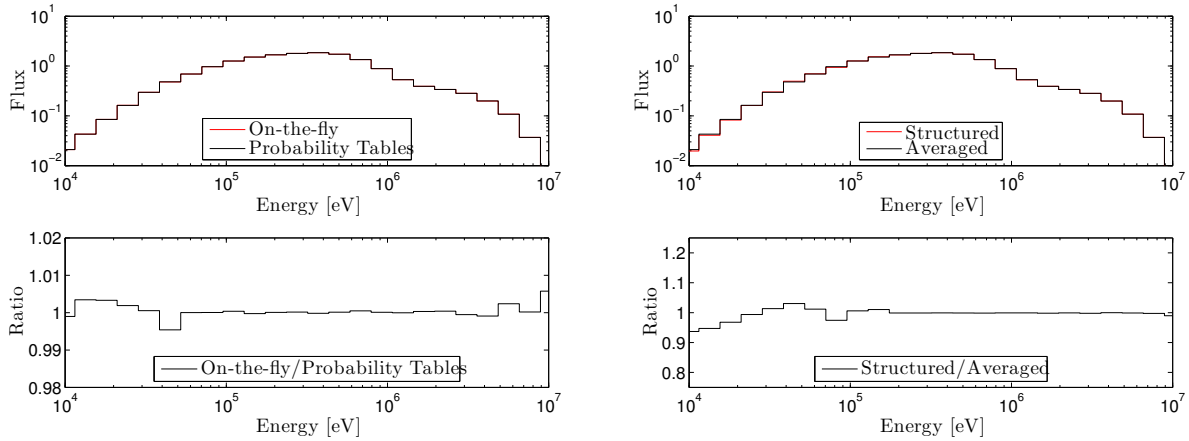

(a) On-the-fly & Probability Tables **(b) Structured & Averaged**

Figure 3. Flux Spectra at 2500 K

3.1.2 Neutron flux energy spectra

Comparisons of flux spectra illustrate the excellent agreement between on-the-fly and probability table results and also the impact of accounting for the resonance structure of the ^{238}U competitive inelastic scattering cross section. Figures 2a and 3a show that — at 293.6 K and 2500 K, respectively — at energies with an appreciable flux, the differential tallies calculated with on-the-fly and probability table cross sections differ by less than one percent. Then, in Figs. 2b and 3b, again for 293.6 K and 2500 K, respectively, we can see the noticeable bias that results when using an averaged, rather than structured, inelastic scattering cross section representation. When using averaged cross sections, inelastic scattering rates in the URR are over-predicted. It follows that flux tallies in the URR and at energies below it are relatively decreased and increased, respectively, compared to the structured cross section case. At energies below the URR, a structured cross section treatment results in flux tally values that are reduced by approximately 5-10% from the values computed with averaged cross sections.

3.2 Big Ten Critical Assembly

The second system that we investigate is the ICSBEP *improved model* of the Big Ten critical assembly. A real system with an intermediate/fast spectrum, Big Ten highlights the same key phenomena that are observed in the infinite, homogeneous medium test problem results. Where indicated, an on-the-fly treatment is applied to only ^{238}U with structured URR cross sections for the other nuclides coming from probability tables.

3.2.1 k_{eff} eigenvalues

Table III gives the k_{eff} results for different URR cross section treatments. We see that accounting for the resonance structure of URR cross sections, with either probability tables or on-the-fly calculations, results in a ~ 400 pcm increase in k_{eff} relative to the case in which averaged cross sections are utilized. Modeling the resonance structure of the ^{238}U first level inelastic scattering reaction cross section contributes another ~ 40 pcm increase. Finally, we see agreement to within a 10 pcm 1σ value between the probability table and on-the-fly eigenvalues.

Table III. Comparison of k_{eff} for Various URR Treatments

URR Method	Inelastic Cross Section	k_{eff}	1σ
Averaged	Averaged	1.00082	0.00010
Probability tables	Averaged	1.00467	0.00010
On-the-fly	Averaged	1.00462	0.00009
On-the-fly	Structured	1.00503	0.00010

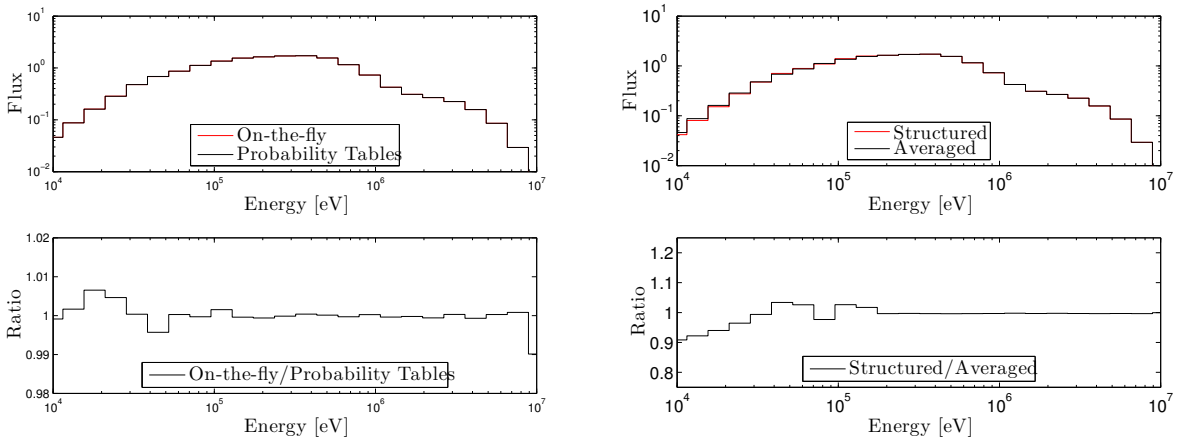

(a) On-the-fly & Probability Tables **(b) Structured & Averaged**

Figure 4. Big Ten Flux Spectra

3.2.2 Neutron flux energy spectra

As in the infinite, homogeneous test problem case, excellent agreement is observed between on-the-fly and probability table differential flux spectra. The largest differences at energies with an appreciable flux are less than one percent. When inelastic scattering cross section resonance structure is introduced into the URR treatment, there is a non-negligible decrease in flux of up to 10% at lower energies due to the reduced inelastic scattering rate in the URR, relative to the averaged cross section case. This is precipitated by an increased flux within the URR which is also due to the reduced inelastic scattering rate. In other words, less URR inelastic scattering in the structured cross section case means that neutrons are transferred less frequently from the URR to lower energies which translates to increased and decreased flux in the URR and below it, respectively.

4 CONCLUSIONS AND FUTURE WORK

The work presented in this initial study demonstrates a procedure for computing URR cross sections on-the-fly in Monte Carlo neutron transport codes, without reliance on a pre-processing step, such as probability table generation. Excellent agreement — within 2σ for relatively tight statistical uncertainties — is observed in comparisons of both integral and differential tallies that are calculated using the on-the-fly method with those obtained using probability tables. This is achieved in simulations of two intermediate spectrum systems which are highly sensitive to URR resonance effects.

With respect to runtime, the computational expense of calculating URR cross sections on-the-fly in the course of a simulation may be relatively severe, or quite manageable, relative to the probability table method, depending on the type of simulation. For example, in a basic criticality simulation of the ICSBEP Big Ten assembly model, with only a k_{eff} tally, the on-the-fly method, when applied to a single important nuclide, is observed to run 10-20 times slower than the probability table method. However, in a simulation with more complex tallies, similar to those that may be required in practical fast reactor analysis simulations, the runtime overhead associated with the on-the-fly

method is reduced to 10-20%[¶]. Longer runtimes can be expected when the on-the-fly method is applied to more nuclides. However, this impact will be reduced, in a relative sense, if reaction rate tallies of practical complexity are calculated in the simulation. Additional reductions in runtime overhead will be realized once optimizations of the on-the-fly algorithm are explored. Further quantification of the method's impact on runtime is necessary in order to establish its viability for both simple criticality calculations and detailed fast reactor analysis.

Because on-the-fly computations rely on temperature-independent unresolved resonance parameters rather than probability tables of arbitrary number and size, memory reduction is achieved with the method. For example, the probability tables for the four nuclides in the Big Ten model account for 71 kB per temperature while the unresolved resonance parameter data needed for on-the-fly calculations take up only 16 kB, total, independent of the number of temperatures. For this reason, even greater memory reductions are attainable in simulations with transient or spatially-varying temperatures because probability table data are likely to be required at several temperatures to ensure that interpolation errors are sufficiently small whereas the on-the-fly method allows for the calculation of cross sections continuously in temperature from a single set of unresolved resonance parameters. Also, there are URR resonance parameters given for 269 of the 423 nuclides in the ENDF/B-VII.1 evaluated data. In systems containing more of these nuclides, further memory reductions will be realized with the on-the-fly method relative to probability tables. Additional quantification of the memory reductions that are achievable with the on-the-fly method is planned.

5 ACKNOWLEDGMENTS

This material is based upon work supported under the first author's appointment to a Department of Energy Nuclear Energy University Programs Graduate Fellowship. This research is also supported in part by the Consortium for Advanced Simulation of Light Water Reactors (CASL), an Energy Innovation Hub for Modeling and Simulation of Nuclear Reactors under U.S. Department of Energy Contract No. DE-AC05-00OR22725.

6 REFERENCES

[1] A. T. Pavlou and W. Ji, "On-the-Fly Sampling of Temperature-Dependent Thermal Neutron Scattering Data for Monte Carlo Simulations," *Ann. Nucl. Energy*, **71**, pp. 411–426 (2014).

[2] G. Yesilyurt, W. Martin, and F. Brown, "On-The-Fly Doppler Broadening for Monte Carlo Codes," *Nucl. Sci. Eng.*, **171**, pp. 239–257 (2012).

[3] T. Viitanen and J. Leppänen, "Explicit Treatment of Thermal Motion in Continuous-Energy Monte Carlo Tracking Routines," *Nucl. Sci. Eng.*, **171**, pp. 165–173 (2012).

[4] B. Forget, S. Xu, and K. Smith, "Direct Doppler Broadening in Monte Carlo Simulations Using the Multipole Representation," *Ann. Nucl. Energy*, **64**, pp. 78–85 (2014).

[5] A. Foderaro, *The Elements of Neutron Interaction Theory*, MIT Press (1971).

[6] R. D. Mosteller and R. C. Little, "Impact of MCNP Unresolved Resonance Probability-Table Treatment on Uranium and Plutonium Benchmarks," LA-UR-98-2943, Los Alamos National Laboratory (1998).

[¶]The referenced simulation consists of absorption, fission, and energy production tallies for each of four nuclides in one hundred equal-lethargy bins across a regular spatial mesh with 30 cells along each axis sized to just cover the entire assembly.

[7] L. Levitt, "The Probability Table Method for Treating Unresolved Neutron Resonances in Monte Carlo Calculations," *Nucl. Sci. Eng.*, **49**, pp. 450–457 (1972).

[8] T. M. Sutton and F. B. Brown, "Implementation of the Probability Table Method in a Continuous-Energy Monte Carlo Code System," *International Conference on the Physics of Nuclear Science and Technology*, vol. 2, p. 891, Long Island, New York, October 5-8, 1998.

[9] M. Dunn and L. Leal, "Calculating Probability Tables for the Unresolved-Resonance Region Using Monte Carlo Methods," *Nucl. Sci. Eng.*, **148**, pp. 30–42 (2004).

[10] R. MacFarlane and A. Kahler, "Methods for Processing ENDF/B-VII with NJOY," *Nucl. Data Sheets*, **111**, pp. 2739–2890 (2010).

[11] A. Trkov, M. Herman, and D. Brown, "ENDF-6 Formats Manual," BNL-90365-2009 Rev.2, National Nuclear Data Center, Brookhaven National Laboratory (2012).

[12] R. E. MacFarlane, R. M. Blomquist, D. E. Cullen, E. Lent, and J. C. Sublet, "A Code Comparison Study for the Bigten Critical Assembly," LA-UR-08-4668, Los Alamos National Laboratory (2008).

[13] Tripoli-4 Project Team, 2008, "Tripoli-4 User Guide," CEA-R-6169, French Alternative Energies and Atomic Energy Commission (2008).

[14] J. C. Sublet, P. Ribon, and M. Coste-Delclaux, "CALENDF-2010: User Manual," CEA-R-6277, French Alternative Energies and Atomic Energy Commission (2011).

[15] X-5 Monte Carlo Team, "MCNP – A General Monte Carlo N-Particle Transport Code, Version 5," LA-UR-03-1987, Los Alamos National Laboratory (2008).

[16] R. Macfarlane and D. Muir, "The NJOY Nuclear Data Processing System, Version 91," LA-12740-M, Los Alamos National Laboratory (1994).

[17] P. Romano and B. Forget, "The OpenMC Monte Carlo Particle Transport Code," *Ann. Nucl. Energy*, **51**, pp. 274–281 (2013).

[18] F. Fröhner, "Applied Neutron Resonance Theory," KfK 2669, Institute for Neutron Physics and Reactor Technology, Karlsruhe Nuclear Research Center (1978).

[19] G. Breit and E. Wigner, "Capture of Slow Neutrons," *Phys. Rev.*, **49**, pp. 519–531 (1936).

[20] D. Cullen and C. Weisbin, "Exact Doppler Broadening of Tabulated Cross Sections," *Nucl. Sci. Eng.*, **60.3**, pp. 199–229 (1976).

[21] G. I. Bell and S. Glasstone, *Nuclear Reactor Theory*, Division of Technical Information, United States Atomic Energy Commission (1970).

[22] G. Hansen and H. Paxton, "A Critical Assembly of Uranium Enriched to 10% in Uranium-235," *Nucl. Sci. Eng.*, **72**, pp. 230–236 (1979).

[23] NEA Nuclear Science Committee, "International Handbook of Evaluated Criticality Safety Benchmark Experiments," NEA/NSC/DOC(95)03, OECD Nuclear Energy Agency (2013).

[24] J. L. Conlin et al., "Continuous Energy Neutron Cross Section Data Tables Based upon ENDF/B-VII.1," LA-UR-13-20137, Los Alamos National Laboratory (2013).

[25] M. Chadwick et al., "ENDF/B-VII.1 Nuclear Data for Science and Technology: Cross Sections, Covariances, Fission Product Yields and Decay Data," *Nucl. Data Sheets*, **112**, pp. 2887–2996 (2011).

APPENDIX A VARIABLE NOTATION

Variable	Symbol
Lab system incident neutron energy	E_n
Lab system neutron resonance energy	E_λ
Shifted lab system neutron resonance energy	E'_λ
Orbital angular momentum	l
Total angular momentum	J
Nuclear spin	I
Statistical spin factor	g_J
Elastic scattering cross section	σ_n
Radiative capture cross section	σ_γ
Fission cross section	σ_f
Competitive reaction cross section	σ_x
Resonance peak cross section	σ_λ
Potential scattering cross section	σ_{pot}
Mean level spacing	$\langle D^{l,J} \rangle$
Sampled level spacing	$D^{l,J}$
Mean reduced neutron width	$\langle \Gamma^{l,J}_{n,0} \rangle$
Sampled neutron width	$\Gamma^{l,J}_n$
Mean radiative capture width	$\langle \Gamma^{l,J}_\gamma \rangle$
Sampled radiative capture width	$\Gamma^{l,J}_\gamma$
Mean fission width	$\langle \Gamma^{l,J}_f \rangle$
Sampled fission width	$\Gamma^{l,J}_f$
Mean competitive reaction width	$\langle \Gamma^{l,J}_x \rangle$
Sampled competitive reaction width	$\Gamma^{l,J}_x$
Total resonance width	Γ_λ
Neutron width degrees of freedom	$\mu^{l,J}_n$
Radiative capture width degrees of freedom	$\mu^{l,J}_\gamma$
Fission width degrees of freedom	$\mu^{l,J}_f$
Competitive reaction width degrees of freedom	$\mu^{l,J}_x$
Channel radius	a_c
Scattering radius	a_s
Center-of-mass neutron wavenumber	k
Penetration factor	P_l
Hard-sphere phase shift	ϕ_l
Shift factor	S_l
Target nuclide material temperature	T
Boltzmann constant	k_{B}